AIP | Physics of Plasmas

# Vlasov multi-dimensional model dispersion relation

Pavel M. Lushnikov, Harvey A. Rose, Denis A. Silantyev, and Natalia Vladimirova

Citation: Physics of Plasmas (1994-present) **21**, 072103 (2014); doi: 10.1063/1.4886122
View online: http://dx.doi.org/10.1063/1.4886122
View Table of Contents: http://scitation.aip.org/content/aip/journal/pop/21/7?ver=pdfcov
Published by the AIP Publishing



# Vlasov multi-dimensional model dispersion relation

Pavel M. Lushnikov,[1,a)] Harvey A. Rose,[2,3] Denis A. Silantyev,[1,3] and Natalia Vladimirova[1,3]
[1]*Department on Mathematics and Statistics, University of New Mexico, Albuquerque, New Mexico 87131, USA*
[2]*Theoretical Division, Los Alamos National Laboratory, MS-B213, Los Alamos, New Mexico 87545, USA*
[3]*New Mexico Consortium, Los Alamos, New Mexico 87544, USA*

(Received 8 December 2013; accepted 16 June 2014; published online 2 July 2014)

A hybrid model of the Vlasov equation in multiple spatial dimension $D > 1$ [H. A. Rose and W. Daughton, Phys. Plasmas **18**, 122109 (2011)], the Vlasov multi dimensional model (VMD), consists of standard Vlasov dynamics along a preferred direction, the $z$ direction, and $N$ flows. At each $z$, these flows are in the plane perpendicular to the $z$ axis. They satisfy Eulerian-type hydrodynamics with coupling by self-consistent electric and magnetic fields. Every solution of the VMD is an exact solution of the original Vlasov equation. We show approximate convergence of the VMD Langmuir wave dispersion relation in thermal plasma to that of Vlasov-Landau as $N$ increases. Departure from strict rotational invariance about the $z$ axis for small perpendicular wavenumber Langmuir fluctuations in $3D$ goes to zero like $\theta^N$, where $\theta$ is the polar angle and flows are arranged uniformly over the azimuthal angle. © *2014 AIP Publishing LLC*. [http://dx.doi.org/10.1063/1.4886122]

## I. INTRODUCTION

Multi-dimensional simulations of the Vlasov equation[1] are possible,[2] but present a significant computational burden compared to particle in cell (PIC) methods.[3,4] However, there are regimes when PIC simulations are challenging. For example, it was found[5,6] that a large number of PIC simulation particles (in 2D, typically the order of 512 particles per Debye length squared) are required near the stimulated Raman scatter (SRS) threshold,[7] to ensure that the time average reflectivity is not sensitive to a further increase of particle number. This relatively large number of particles is required to suppress artificial "particle noise" in PIC simulations to the point, where its unphysical contribution to the loss of electrons, trapped in the SRS daughter Langmuir wave (LW), is a correction to the physically dominant detrapping mechanism. Since the latter is regime dependent, e.g., electron-ion collision dominant regime versus a laser speckle side loss dominant regime versus a rapidly varying SRS regime, a priori estimates as to what constitutes a sufficient number of particles are not reliable and one must perform a convergence study[7] by adding more and more simulation particles. Other regimes, where PIC simulations are challenging include instability onset, which is also sensitive to noise levels. In particular, the Langmuir wave decay instability is easily disrupted by ion noise.[8]

Modeling the Vlasov equation as a fluid is inadequate for linear regimes in which Landau damping[9] and, nonlinearly, e.g., electron trapping by LWs, are significant. However, if plasma wave propagation is largely confined to a narrow cone about the $z$ axis, as may be the case for SRS;[10–12] then, these kinetic effects may be adequately described by a recently developed kinetic-fluid hybrid Vlasov multi dimensional model (VMD),[13] consisting of standard Vlasov dynamics along the $z$ direction and $N$ fluid flows with velocities $\{\mathbf{u}_i(x,y,z,t)\}_{i=1\ldots N}$ in the $xy$ (perpendicular) plane with the corresponding flow densities $\{\rho_i(x,y,z,t)\}_{i=1\ldots N}$. These flows are coupled by self-consistent electric and magnetic fields. Each flow convects its corresponding one-dimensional ($1D$) distribution function, $\{f_i(x,y,z,v_z,t)\}_{i=1\ldots N}$, in the $xy$ plane.

In Ref. 13, the only case considered in detail was two-dimensional ($2D$) case with two transverse flows ($N=2$). Here, we address several key issues, which were not addressed in Ref. 13. We consider both a $2D$ case with only one transverse direction, $x$, taken into account as well as a fully $3D$ case with two transverse directions $x$ and $y$. First, we analyze in $2D$ whether or not the VMD Langmuir wave dispersion relation converges to that of the original Vlasov equation with addition of more transverse flows (beyond two transverse flows of Ref. 13), i.e., we consider $N > 2$. We find that with increase of $N$, the VMD Langmuir wave dispersion relation approximately converges to that of the Vlasov equation with the relative error $\sim 10^{-3}$ for the typical values of the parameters. This accuracy deteriorates rapidly as $k\lambda_D$ decreases below $\sim 0.2$, where $\lambda_D$ is the Debye length and $k$ is the LW wavenumber. Since as shown in Ref. 14, trapped electron effects, such as frequency shift, rapidly decrease in magnitude for $k\lambda_D < 0.2$, the VMD is most useful in the complementary "kinetic regime," $k\lambda_D > 0.2$. Second, we investigate that the choice of initial velocities $\{\mathbf{u}_i\}_{i=1\ldots N}$ and associated densities $\{\rho_i\}_{i=1\ldots N}$ is optimal with regard to accuracy of the LW dispersion relation of the Vlasov equation. Third, we identify how the range of propagation angle, $\theta$, for which all modes are stable, changes with increase of $N$. Fourth, we analyzed the three-dimensional ($3D$) case to find the number of flows required to qualitatively represent the LW filamentation instability. Rotational invariance about the $z$ axis is not strictly satisfied by VMD. However, we show that the discrepancy with strict rotational invariance for small perpendicular wavenumber Langmuir fluctuations in $3D$ goes to zero $\propto \theta^N$ provided that the flows are arranged uniformly over the azimuthal angle. Here, $\theta$ is the polar angle. In

a)plushnik@math.unm.edu

 

particular, we find that the minimum value of $N=6$ is consistent with isotropic filamentation instability. Fifth, we verify that the VMD recovers the properties of small amplitude traveling wave solutions, which are Bernstein-Greene-Kruskal (BGK) modes.[15] Sixth, we go beyond linear analysis by performing fully nonlinear VMD simulations, whose results are compared with 2*D* Vlasov simulations.

The paper is organized as follows. In Sec. II, we recall the basic properties of VMD. In Sec. III, we analyze the increase of VMD accuracy with increase of the number of flows $N$ as well as the boundaries of stability. In Sec. IV, the properties of 3*D* VMD dispersion relation are studied. Section V discusses the application of VMD to nonlinear waves and recovery of BGK modes properties by VMD. In Sec. VI, we present fully nonlinear VMD simulation results with conditions similar to the Vlasov simulations of Ref. 2. In Sec. VII, the main results of the paper are discussed.

## II. VMD MODEL REDUX

In this Section, the VMD basic properties[13] are recalled. Let $g$ be a particular species' phase space distribution function. The VMD ansatz is

$$g(\mathbf{x},\mathbf{v},t)=\sum_{i=1}^{N} f_i(\mathbf{x},v_z,t)\delta(\mathbf{v}_\perp-\mathbf{u}_{i\perp}(\mathbf{x},t)). \tag{1}$$

Here, 3*D* position and velocity vectors are denoted by $\mathbf{x}$ and $\mathbf{v}$, respectively, and the latter may represented by its perpendicular (*xy* plane), $\mathbf{v}_\perp$, and parallel (the $z$ axis) projections, $v_z$

$$\mathbf{v}=\mathbf{v}_\perp+v_z\hat{\mathbf{e}}_z,\quad \mathbf{v}_\perp\cdot\hat{\mathbf{e}}_z=0, \tag{2}$$

with $\hat{\mathbf{e}}_z$ being the unit vector along the $z$ axis. The Vlasov equation, in units such that electron mass and charge are normalized to unity and $\mathbf{v}$ is normalized to the electron thermal speed $v_e$, is

$$\left\{\frac{\partial}{\partial t}+\mathbf{v}\cdot\nabla+\mathbf{E}\cdot\frac{\partial}{\partial\mathbf{v}}\right\}g=0, \tag{3}$$

where $\mathbf{E}$ is the electric field. Magnetic field effects are ignored for clarity. It can be shown[13] that Eqs. (1) and (3) imply

$$\left\{\frac{\partial}{\partial t}+v_z\frac{\partial}{\partial z}+E_z\frac{\partial}{\partial v_z}\right\}f_i+\nabla_\perp\cdot(\mathbf{u}_{i\perp}f_i)=0, \tag{4}$$

$$\left\{\frac{\partial}{\partial t}+\mathbf{u}_i\cdot\nabla\right\}\mathbf{u}_{i\perp}=\mathbf{E}_\perp. \tag{5}$$

Flow fields $\mathbf{u}_i$ are decomposed similar to Eq. (2) as

$$\mathbf{u}_i=\mathbf{u}_{i\perp}+u_{iz}\hat{\mathbf{e}}_z,\quad \mathbf{u}_{i\perp}\cdot\hat{\mathbf{e}}_z=0,\quad i=1\ldots N \tag{6}$$

with their perpendicular components determined by Eq. (5) and its $z$ component by

$$\rho_i u_{iz}=\int v_z f_i(\mathbf{x},v_z,t)dv_z, \tag{7}$$

where

$$\rho_i=\int f_i(\mathbf{x},v_z,t)dv_z \tag{8}$$

is the $i$th flow's density.

The electric field $\mathbf{E}$ is determined by the total density $\rho=\sum_{i=1}^{N}\rho_i$ together with Poisson's equation. Recall that the summation over $i$ is a sum over flow field components for a given species. An additional sum over species is required to obtain the total charge and current densities but below we assume a single specie plasma for simplicity. Equations (4) and (5) constitute the VMD model. VMD solutions, for wave propagation strictly along the $z$ axis, are precisely correct because, in this case, the VMD model coincides with the Vlasov equation.

In the electrostatic regime

$$\mathbf{E}=-\nabla\phi, \tag{9}$$

with Poisson's equation

$$\nabla^2\phi=-\rho, \tag{10}$$

where $\phi$ is the electrostatic potential and the factor $4\pi$ is absent in (10) because we normalize length to the electron Debye length, and frequency to the electron plasma frequency.[13]

In Ref. 13, it was shown that the VMD model's basic limitation in 2*D* with $N=2$ is the restriction to wave propagation dominantly along the $z$ axis to avoid an unphysical two-stream-instability. These results are recalled and extended to large values of $N$ in Sec. III.

## III. INCREASE OF ACCURACY WITH FLOW NUMBER IN 2D

In 2D, for the minimal $N=2$ case, linearizing Eqs. (4), (5), (9), and (10) around the thermal equilibrium distribution function $f_0$

$$g_0=\frac{1}{2}[\delta(v_x-u)+\delta(v_x+u)]f_0(v_z),$$
$$f_0(v)=\frac{1}{\sqrt{2\pi}}\exp\left(-\frac{v^2}{2}\right), \tag{11}$$

with a perturbation $\propto\exp(i\mathbf{k}\cdot\mathbf{x}-i\omega t)$, one obtains VMD dispersion relation for a fluctuation with wavenumber $k=|\mathbf{k}|$, making an angle $\theta$ with respect to the $z$ axis

$$4k^2=Z'(\zeta_+)+Z'(\zeta_-)$$
$$-\tan^2(\theta)\left(\frac{Z(\zeta_+)}{\zeta_+}+\frac{Z(\zeta_-)}{\zeta_-}\right),$$
$$\zeta_\pm=\frac{\mp u\sin(\theta)+\omega/k}{\sqrt{2}\cos(\theta)},$$
$$Z(\zeta)=\frac{1}{\sqrt{\pi}}\int_{-\infty}^{+\infty}\frac{\exp(-t^2)}{t-\zeta}dt, \tag{12}$$

where $Z$ is the plasma dispersion function.[16]

In comparison, linearization of the Vlasov equation (3) with (9) and (10) around $f_0$ (11) results in the dispersion relation

$$4k^2\cos^2(\theta) = Z'(\zeta_+) + Z'(\zeta_-), \tag{13}$$

where $\zeta_\pm$ are defined in (12).

The VMD dispersion relation (12) coincides with the Vlasov equation dispersion relation (13) in two limiting cases when $\theta \to 0$ and $\theta \to \pi/2$. In the case of $\theta \to 0$, the VMD dispersion relation coincides with the Vlasov dispersion relation for isotropic thermal plasma

$$2k^2 = Z'(v_\varphi/\sqrt{2}), \tag{14}$$

where $v_\varphi \equiv \omega/k$ is the phase velocity. And in the second case of $\theta \to \pi/2$, we obtain the well-known cold plasma two-stream dispersion relation[17]

$$2 = \frac{1}{(\omega - uk)^2} + \frac{1}{(\omega + uk)^2}. \tag{15}$$

It has been shown[13] that the LW dispersion relation (14) is qualitatively recovered in the VMD dispersion relation (12) for $u \approx 1$ and angle of propagation between the $z$ axis and wave-vector $\mathbf{k}$, $\theta \lesssim 0.65$, beyond which a variant of the two-stream instability is encountered. This region of instability is an artifact of the two-stream model, Eq. (11). Here, we demonstrate that an increase of $N$ in $2D$ has a stabilizing effect.

To emulate thermal equilibrium, with $N$ transverse flows, $\{u_i\}_{i=1\ldots N}$, it is natural to choose their weights, $\{\rho_i\}_{i=1\ldots N}$, proportional to that of true thermal equilibrium

$$g_0(v_x, v_z) = f_0(v_z)\sum_{i=1}^{N}\rho_i\delta(v_x - u_i),$$
$$\sum_{i=1}^{N}\rho_i = 1, \quad \rho_i \sim \exp\left(-\frac{u_i^2}{2}\right), \tag{16}$$

so that the total density, $\rho$, is normalized to unity. The apparent factorization implies independence of $v_z$ and $v_x$ fluctuations, as in true thermal equilibrium. We employ the symmetry about $v_x = 0$ and use one additional restriction that must be imposed to have a unit mean square transverse velocity

$$\sum_{i=1}^{N}\rho_i u_i^2 = 1, \tag{17}$$

so that the transverse and $z$-direction temperatures coincide. Criteria for choosing $u$ for $N = 2$, Eq. (11), were presented in Ref. 13. Here, we emphasize $N \gg 1$ results. The general VMD dispersion relation for $2D$ case with $N \geq 2$ is

$$2k^2 = \sum_{i=1}^{N}\rho_i\left(Z'(\zeta_i) - \tan^2(\theta)\frac{Z(\zeta_i)}{\zeta_i}\right),$$
$$\zeta_i = \frac{-u_i\sin(\theta) + \omega/k}{\sqrt{2}\cos(\theta)}. \tag{18}$$

One reasonable flow requirement is a recovery of standard Landau damping in the linear regime and the other one is to ensure a maximum region of stability. Recall, the test-particle point of view of Dawson[18] for Landau damping, where an electron with a LW's phase velocity $v_\varphi$ interacts with the wave for a finite time. However, for the VMD to recover a LW's Landau damping, $\nu_L$, it is sufficient (but not necessary, see Fig. 3 in Ref. 13) that its phase velocity is close to a kinematically accessible one, as in Fig. 1, which illustrates a plane wave sinusoidal electric field, with wavenumber $k$, phase velocity $v_\varphi$, propagating at an angle $\theta$ with the $z$ axis, and whose $x$ velocity projection, $v_{\varphi x} = v_\varphi\sin(\theta)$, lies in the interval $(u_i, u_{i+1})$. Typically, $v_\varphi$ will not coincide with a particular $u_i$, rather, a test particle horizontal velocity will differ from precise resonance with the wave by order $\Delta u_i \equiv u_{i+1} - u_i$ causing its location to dephase with the wave in a time scale $\sim 1/[k\Delta u_i\sin(\theta)]$. To obtain a qualitatively faithful rendition of Landau damping, this must be large compared to a Landau damping time, or equivalently

$$k\Delta u_i\sin(\theta) \ll 2\pi\nu_L. \tag{19}$$

Besides the two general constraints (16) and (17), we consider the VMD dispersion relation (18) in two ways: (a) we find range of parameters when (18) gives only stable solutions and (b) we compare solutions of the LW branch of the VMD dispersion relation (18) with the exact result for the LW branch of the Vlasov equation dispersion relation (14).

We choose a flow spacing, $\Delta u = |u_{i+1} - u_i|$, which is independent of flow index, $i$. We decrease $\Delta u$ with increase of $N$ as follows. Consider $N$ flows $u_i$ evenly spaced between $-U_{max}$ and $U_{max}$, skipping $u = 0$. Take a positive integer $n$ and choose

$$U_{max} = n, \quad \Delta u = 1/2^{n-1}, \quad N = n2^n. \tag{20}$$

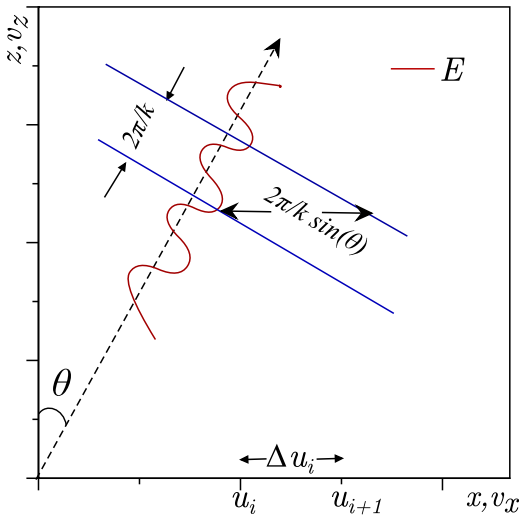


FIG. 1. Cartoon of electric field, red oscillatory curve, and phase fronts, blue lines, illustrates possible electron de-phasing. A VMD electron typically has a velocity difference in $v_x$ direction with the wave's, $v_\varphi\sin(\theta)$, of order $\Delta u_i$ and will dephase in a time of order $2\pi/[k\Delta u_i\sin(\theta)]$.

According to Eq. (20), with increase of $n$, $U_{max}$ grows linearly, $\Delta u$ decreases exponentially and $N$ grows faster by a factor $n$ than the exponential growth $2^n$.

(a) The stability boundary of the VMD dispersion relation (18) is shown in Fig. 2 for $N=2$, 8, 24, and 64 ($n=1$, 2, 3, 4). For each given $N$, the region below the corresponding curve has only stable modes $Im(\omega)\le 0$ and above the curve there is at least one unstable solution $Im(\omega)>0$. While the area of the unstable region increases (but converges) with increase of $N$, the maximum growth rate $\max Im(\omega)$ decreases as $1/N^{\alpha}$, with $\alpha\approx 0.5$ for the above scheme (20). For this family of flows, the most unstable roots of (18) for $\theta\neq 0$ correspond to $Re(\omega)\approx 0$. These unstable roots move as $k$ and $\theta$ are changed. The stability boundary is obtained by finding numerically $k$ such that for each given $\theta$, the most unstable solution (the solution with the largest positive value of $Im(\omega)$ for given $k$ and $\theta$) of the dispersion relation turns into $\mathrm{Im}(\omega)=0$. The solutions of (18) corresponding to the Langmuir wave are stable for any choice of $k$ and $\theta$. From practical point of view of VMD simulations, we filter out at each time step, whose perturbations with $\theta>\theta_{max}\simeq 0.65$, which ensures that we stay inside the stable region of Figure 2 for any $k$. If initially, there is not much energy near the angular cutoff, $\theta_{max}$, but VMD evolution results in significant energy at $\theta_{max}$, then, the underlying Vlasov model and VMD solutions are expected to have fundamental differences. In nonlinear VMD simulations of Sec. VI, we did not observe such accumulation near $\theta_{max}$.

(b) Results shown in Figs. 3–5 indicate decreased accuracy of the imaginary part of the LW branch of the VMD dispersion relation (18) as $k\sin(\theta)$ decreases, consistent with the estimate given by Eq. (19), for the case $N=8$, $u_i=[-2, -1.5, -1, -0.5, 0.5, 1, 1.5, 2]$. These Figures show the relative error between the LW branch of the VMD dispersion relation (18) and the exact LW dispersion relation (14) for $\theta=0.1$, 0.3, and 0.5, respectively. The LW branch of VMD dispersion relation for $\theta\neq 0$ is obtained by continuation of the LW branch (14) identified at $\theta=0$. Note that the error in $\mathrm{Im}(\omega)$ (blue solid curves) grows rapidly as $k$ decreases below 0.3, consistent with the rapid decrease of $\nu_L/k$ with decrease of $k$ as shown in Fig. 6. That rapid decrease provides strong constraints on flow spacing, $\Delta u$, and angle of propagation, $\theta$, with respect to the $z$ axis, as per Eq. (19). At the same time, this accuracy decrease occurs mostly for $k<0.2$, where $Im(\omega)$ is exponentially small. But, as shown in Ref. 14, trapped electron effects, such as frequency shift, rapidly decrease in magnitude for $k<0.2$. Thus, the VMD is most useful in the complementary "kinetic regime," $k>0.2$.

Figures 7 and 8 show the relative error between the LW branch of the VMD dispersion relation (18) and the LW dispersion relation (14) on $N$ for a discrete set of values of $N$. It

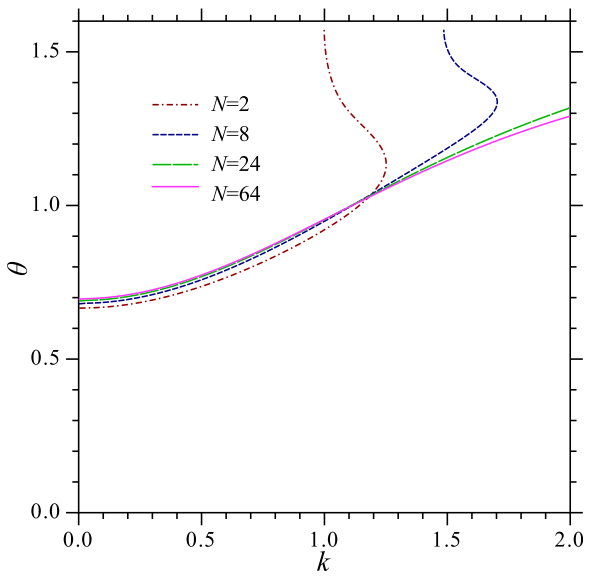


FIG. 2. The stability boundary for the VMD dispersion relation (18) for different numbers of flows, $N$. Stable region is below and to the right of the corresponding curve. As $N$ increases, the stability boundary converges to the universal curve. Above this boundary, instability persists, but growth rate goes to zero as $\sim 1/N^{\alpha}$, with $\alpha\sim 0.5$.

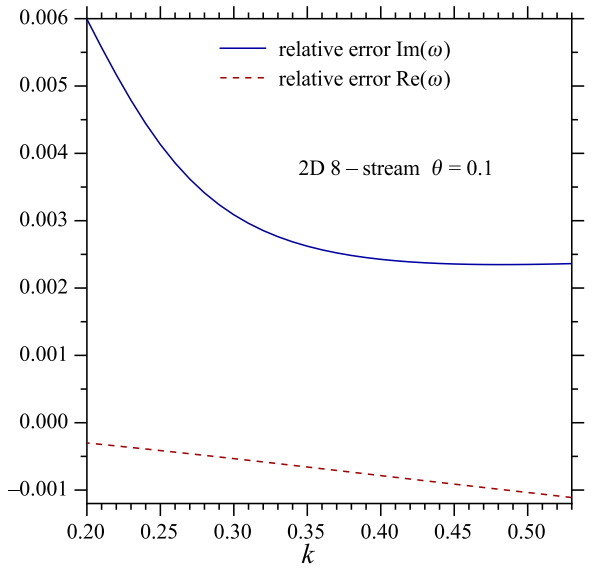


FIG. 3. Relative error between the LW branch of the VMD dispersion relation (18) and the LW dispersion relation (14) for $N=8$ and $\theta=0.1$ as a function $k$.

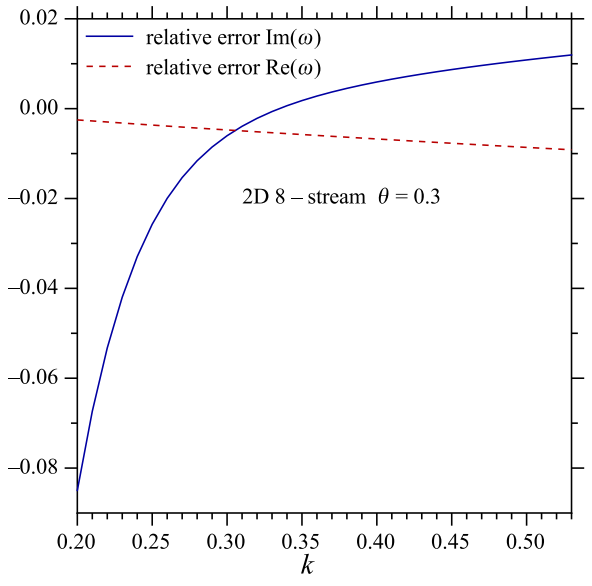


FIG. 4. Relative error between the LW branch of the VMD dispersion relation (18) and the LW dispersion relation (14) for $N=8$ and $\theta=0.3$.

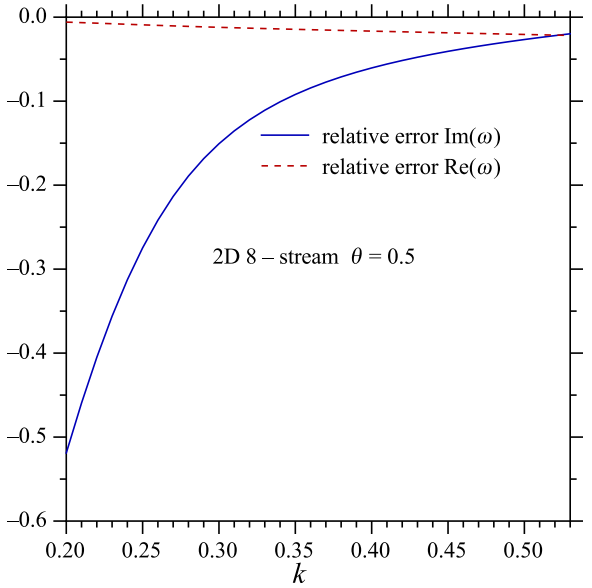


FIG. 5. Relative error between the LW branch of the VMD dispersion relation (18) and the LW dispersion relation (14) for $N=8$ and $\theta=0.5$.

is seen that the relative errors converge for large $N \gg 1$ to the small constants $\sim 10^{-3}$ (for $\theta \sim 0.1$) and $\sim 5\times 10^{-3}$ (for $\theta \sim 0.3$). Thus VMD approximates well LW dispersion relation of Vlasov equation already for $N=2$ and improves that approximation for $N \gg 1$ although a finite error $\sim 10^{-3}$ (for $\theta \sim 0.1$, which is the typical angle, e.g., for simulations of Ref. 2) and $\sim 5\times 10^{-3}$ (for $\theta \sim 0.3$) survives even for $N \to \infty$. It is a limitation of VMD, which cannot be improved with flow discretization given by Eq. (20) but we believe that this relative error is small enough for usefulness of VMD.

## IV. VMD DISPERSION RELATION IN 3D

Consider VMD thermal equilibrium distribution function of the form (11) generalized to 3D with $N$ equally

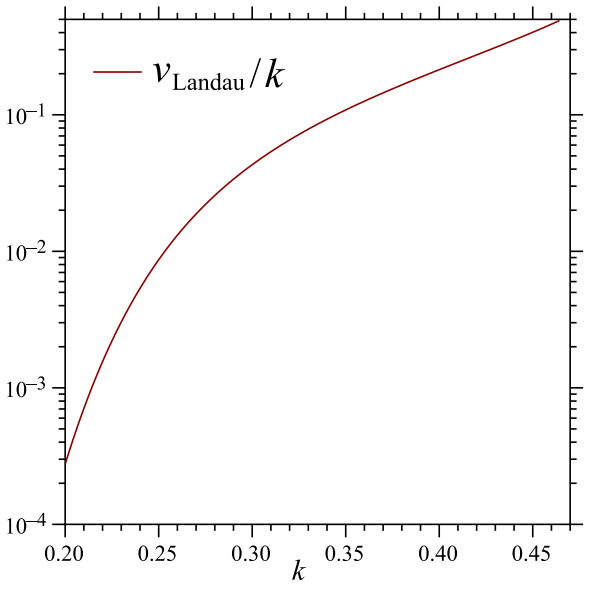


FIG. 6. Dependence of $\nu_L/k$ on $k$ in the LW dispersion relation (14).

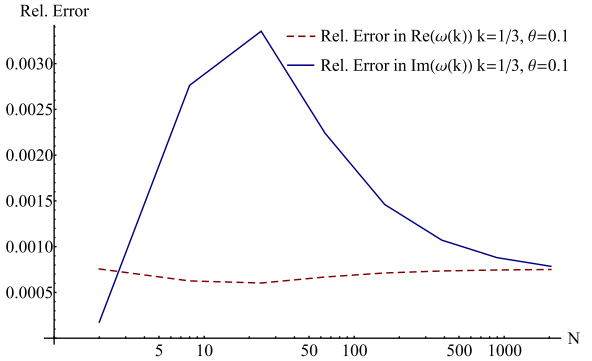


FIG. 7. Dependence of the relative error between the LW branch of the VMD dispersion relation (18) and the LW dispersion relation (14) on $N$ for $k=1/3$ and $\theta=0.1$.

weighted flows in the transverse plane arranged uniformly over the azimuthal angle

$$g_0(\mathbf{v}_\perp, v_z) = \frac{1}{N} f_0(v_z) \sum_{i=1}^{N} \delta(\mathbf{v}_\perp - \mathbf{u}_{i\perp}). \tag{21}$$

The magnitude of $\mathbf{u}_{i\perp}$ for each flow is $\sqrt{2}$, so that $\langle (\mathbf{v}\cdot\mathbf{n})^2 \rangle = 1$ for any $N \geq 3$ independent of the unit vector, $\mathbf{n}$, direction with angular brackets indicating average over the VMD thermal equilibrium state (21). Linearizing Eqs. (4) and (5) around the VMD "thermal equilibrium" distribution function (21), one obtains the $3D$ VMD dispersion relation

$$2Nk^2 = \sum_{i=1}^{N} \left( Z'(\zeta_i) - \tan^2(\theta) \frac{Z(\zeta_i)}{\zeta_i} \right),$$
$$\zeta_i = \frac{-|\mathbf{u}_{i\perp}| \sin(\theta)\cos(\varphi_i - \varphi) + \omega/k}{\sqrt{2}\cos(\theta)}, \tag{22}$$

where $\theta$ and $\varphi$ are polar and azimuthal angle of wave-vector $\mathbf{k}$, respectively, and $\varphi_i = 2\pi i/N$ is azimuthal angle of $i$th flow in transverse plane, as depicted in Figure 9.

Similar to $2D$ case, this dispersion relation coincides with the Vlasov equation dispersion relation in two limiting cases: when $\theta \to 0$ and $\theta \to \pi/2$. In the case of $\theta \to 0$, the VMD dispersion relation coincides with the Vlasov

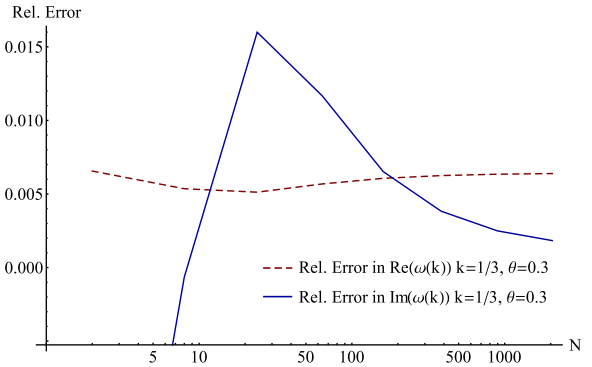


FIG. 8. Dependence of the relative error between the LW branch of the VMD dispersion relation (18) and the LW dispersion relation (14) on $N$ for $k=1/3$ and $\theta=0.3$.

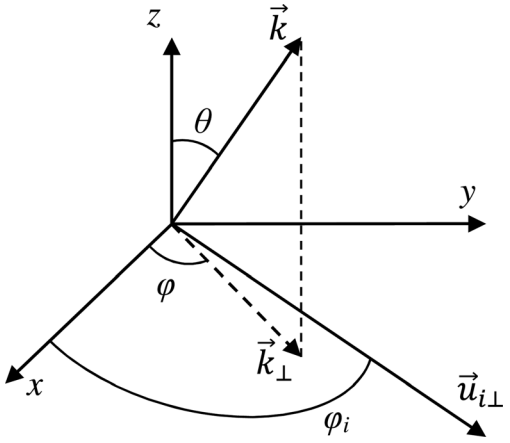


FIG. 9. Schematic 3*D* VMD geometry, with only one of the equilibrium flows, $\mathbf{u}_{i\perp}$, depicted.

dispersion relation for isotropic thermal plasma (14). In the case of $\theta \to \pi/2$, we obtain a generalized two-stream dispersion relation for cold plasma.

$$N = \sum_{i=1}^{N} \frac{1}{(\omega - k|\mathbf{u}_{i\perp}|\cos(\varphi_i - \varphi))^2}. \tag{23}$$

The LW dispersion relation (14) of the Vlasov equation is qualitatively recovered by (22) for $|\mathbf{u}_{i\perp}| = \sqrt{2}$ and $\theta \lesssim 0.65$. Beyond that angle, a variant of the two-stream instability is encountered. Figure 10 shows the stability region envelopes in angle $\varphi$ (the largest unstable cross-section is chosen over all angles $\varphi$) for $N = 4$, 6, 8, 10, and 12. The region below the curves has only stable modes. While the area of the unstable region converges with increase of $N$, the growth rate approximately scales as $C(k, \theta)/N$ for $N \gg 1$. Here, the dependence $C(k, \theta)$ is obtained from simulations. $C(k, \theta)$ attains its maximum at $\theta = \pi/2$ for each fixed $k$. E.g., $C(0.3, \pi/2) \simeq 2.5$. Also

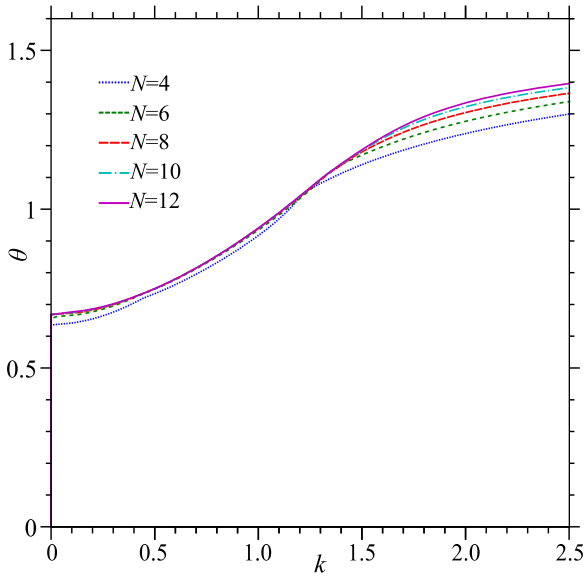


FIG. 10. As the number of flows, $N$, increases, the stability boundary of 3*D* VMD dispersion relation (22) appears to converge. Above this boundary, instability persists, but growth rates go to zero as $\sim 1/N$.

$C(k, \theta) \to 0$ as we approach the stability boundary or $k = 0$ boundary.

The Vlasov dispersion relation (14) is isotropic for thermal plasma. In general, this property is lost for anisotropic equilibria, such as Eq. (21), but it may be approximately regained for small values of the polar angle, $\theta$, for large enough $N$. Based on experience with 2*D* lattice gas models,[19] one expects that six transverse flows, $N = 6$, aligned with the edges of a regular hexagon is sufficient to assure independence of mode properties on the azimuthal angle, $\varphi$, as $\theta \to 0$.

The LW branch, $\omega_{LW}$, of 3*D* VMD dispersion relation (22) depends on wavenumber $k$ as well as the polar and azimuthal angles, $\theta$ and $\varphi$. Figure 11 shows that the maximum excursion of $Re(\omega_{LW})$ as $\varphi$ varies in the interval $0 < \varphi \le \pi/3$, rapidly goes to zero with $\theta$: at any value of $\theta$, this graph depicts the largest magnitude difference $Re(\omega_{LW}(\varphi_1)) - Re(\omega_{LW}(\varphi_2))$ for $0 < \varphi_1, \varphi_2 \le \pi/3$ at $k = 0.3$, normalized to the LW frequency. For equilibrium hexagonal flow geometry, this error varies as $\theta^6$ for small $\theta$, $0 < \theta \le 0.2$, and, since the magnitude of $k$'s projection onto the $xy$ plane, $k_\perp \theta$ for small $\theta$, the error varies as $k_\perp^6$. Similar result can be shown for different numbers of transverse flows $N$ arranged uniformly over the azimuthal angle. Excursion of $\mathrm{Re}(\omega_{LW})$, in this case, varies as $\theta^N$ for small $\theta$.

Figures 12–14 show that, similar to 2*D* case of Sec. III, the LW branch of 3*D* VMD dispersion relation (22) agrees well with the exact Vlasov dispersion relation (14) provided $k \gtrsim 0.3$ and $\theta \lesssim 0.3$. E.g., for $k = 0.35$ with $N = 6$ in 3*D* the relative errors are $\simeq 0.04\%$ for $\theta = 0.1$ and $\simeq 2\%$ for $\theta = 0.3$. We also note that the trapping effects are very small for $k \lesssim 0.2$ but become important at $k \gtrsim 0.3$ with the transition between these regimes at $0.2 \lesssim k \lesssim 0.3$ as can be seen, e.g., in Figure 5 of Ref. 14. Recall also that, in dimensional units, $k$ is replaced by $k\lambda_D$, where $\lambda_D$ is the Debye length.

## V. CONNECTION WITH NONLINEAR WAVES

While this paper's emphasis is primarily linear VMD theory and its comparison with the standard Vlasov equation

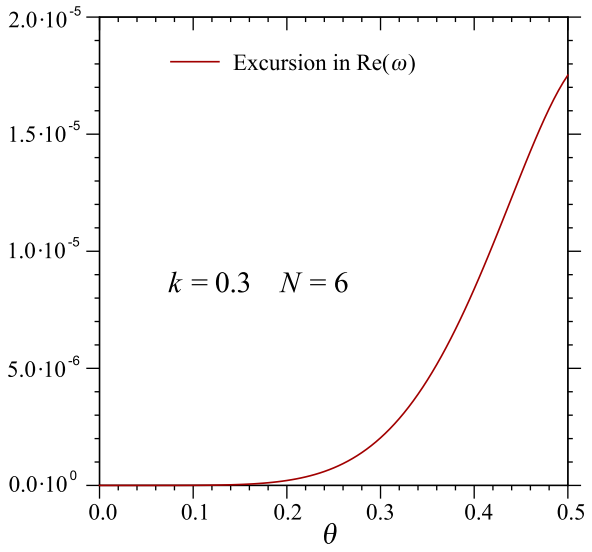


FIG. 11. Excursion in real part of the LW branch of 3*D* VMD dispersion relation (22) with $N = 6$.

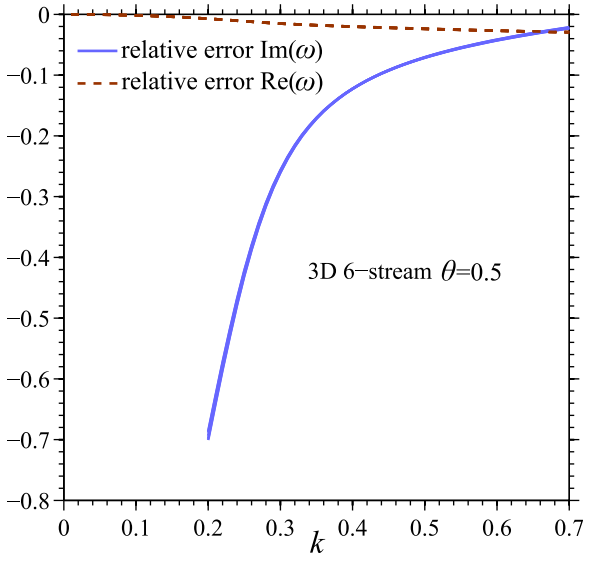


FIG. 12. Relative error between the LW branch of 3D VMD dispersion relation (22) and the LW dispersion relation (14) for $N=6$ and $\theta=0.5$. Several values of the azimuthal angle $\varphi$ are superimposed but they are practically indistinguishable.

dispersion relation (14) results, let us recall the connection with a particular class of small amplitude traveling wave solutions (BGK modes[15]) of the fully nonlinear Vlasov equation: it has been shown[20,21] that these small amplitude BGK modes depend only on the linear susceptibility function $\Xi$, where $\Xi$ is given by the r.h.s. of (14) multiplied by 1/2. $\Xi$ is a function of the phase velocity $v_\varphi = \omega/k$ ($\omega$ is taken here to be real-valued) only. These BGK modes bifurcate from the zeros of the real part of the susceptibility, $Re(\Xi)$, as we allow the wave amplitude to be small but finite (as opposed to vanishing amplitude in the purely linear regime).

The VMD linear susceptibility $\Xi_{VMD}$ is given by r.h.s. of the first in Eq. (22) multiplied by $1/(2N)$. In this case, $\Xi_{VMD}$ is a function of $v_\varphi = \omega/k$, the number of flows, $N$, the flow

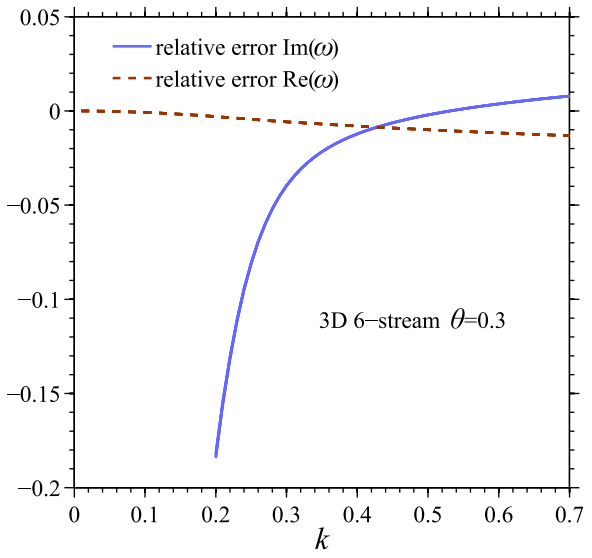


FIG. 13. Relative error between the LW branch of 3D VMD dispersion relation (22) and the LW dispersion relation (14) for $N=6$ and $\theta=0.3$. Several values of the azimuthal angle $\varphi$ are superimposed but they are practically indistinguishable.

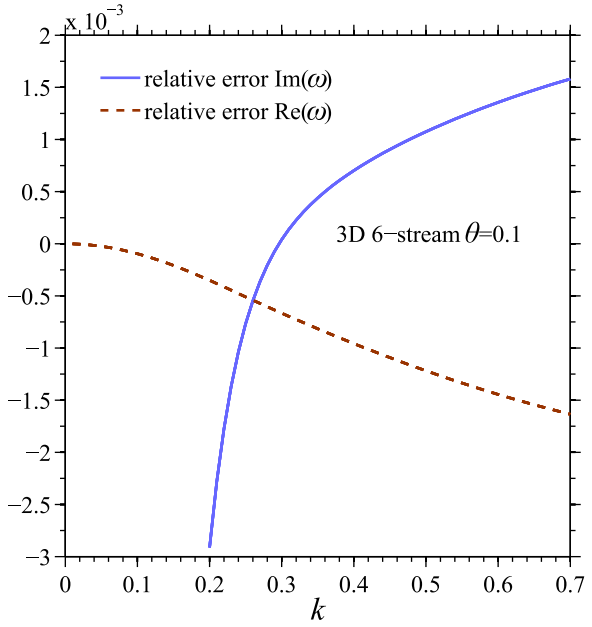


FIG. 14. Relative error between the LW branch of 3D VMD dispersion relation (22) and the LW dispersion relation (14) for $N=6$ and $\theta=0.1$. Several values of the azimuthal angle $\varphi$ are superimposed but they are practically indistinguishable.

locations and the linear wave propagation direction determined by angles $\theta$ and $\varphi$. Figure 15 shows $Re(\Xi_{VMD})$ for $N=6$, $\varphi=0$ and various values of $\theta$. Similar to Figures 12–14, the dependence on the azimuthal angle $\varphi$ is weak. Figure 15 clearly shows that any horizontal line, such as the one shown for $k=0.35$, intersects $Re(\Xi_{VMD})$ in at most two points (two values of $v_\varphi$), which differs only

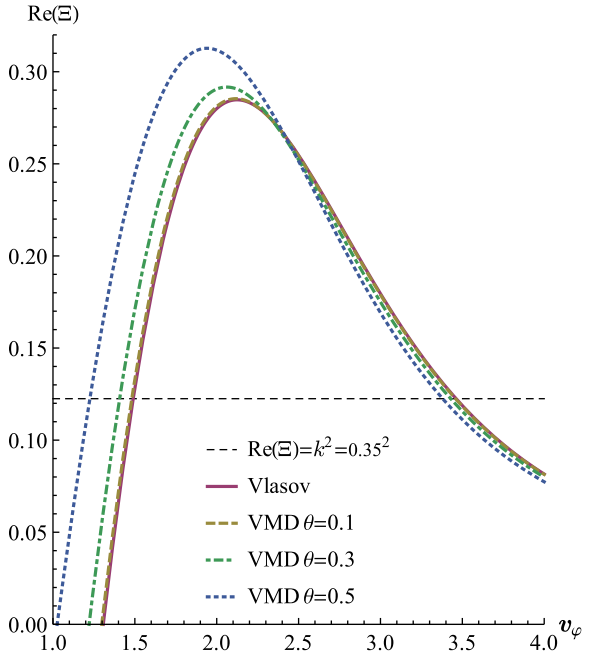


FIG. 15. The linear susceptibility curves $\Xi$ for the Vlasov equation and 3D VMD with $N=6$ at various angles of propagation, $\theta$ vs. phase velocity $v_\varphi = \omega/k$ and $\varphi=0$ with $k=0.35$. The horizontal line at $\Xi=k^2=0.35^2$ intersects a particular susceptibility curve at a phase velocity corresponding to the electron-acoustic wave at $v_\varphi \simeq 1.5$ and the LW at $v_\varphi \simeq 3.5$. In dimensional units, $k$ is replaced by $k\lambda_D$.

quantitatively from the Vlasov equation results (shown by the solid line in Figure 15). The lower $v_\varphi$ intersection corresponds to the electron-acoustic wave, much more damped than the LW and not emphasized in our discussion. The larger $v_\varphi$ intersection corresponds to the LW. There are other linear modes in the sense of Landau (complex zeroes of the dielectric function), but only these two are distinguished in the sense of connecting with small amplitude BGK modes. Comparison with these other linear modes has therefore been ignored in this paper.

We showed in Sec. IV that the departure from isotropy scales as $\theta^N \propto k_\perp^N$, where $k_\perp$ is the transverse wavenumber. It was found in Ref. 22 that the limits of a LW's filamentation instability depend essentially upon hyper-diffraction with the LW's diffraction contribution to its frequency given by $D = D_\perp k_\perp^2 + D_{hyper} k_\perp^4$, where $D_\perp$ and $D_{hyper}$ are diffraction and hyper-diffraction coefficients, respectively. It suggests that one must have $N \geq 6$ in order that the filamentation instability is isotropic with high accuracy.

## VI. NONLINEAR VMD SIMULATIONS IN 2D

To demonstrate the efficiency of VMD, we performed the fully nonlinear simulations of 2D VMD in the conditions similar to the Vlasov simulations of Ref. 2 (one transverse direction $x$). Our numerical code is pseudospectral in all directions (two spatial directions $x$, $z$ and a velocity direction $v_z$) with $0 < z < L_z = 6\pi$, $-L_x/2 < x < L_x/2$, $L_x = 512\pi$, and $-v_{max} < v_z < v_{max}$ with periodic boundary conditions in all directions. We typically used 64 points in $z$, 320 points in $v_z$, 128 points in $x$, and time step $\Delta t = 0.025$. We also performed convergence study by increasing number of points and decreasing $\Delta t$. We used large enough $v_{max}$ (typically, we chose either $v_{max} = 6.25$ or $v_{max} = 7.25$) to avoid influence of periodicity over $v_z$ in comparison with the decay $\propto e^{-v_z^2/2}$ for $|v_z| \to \infty$. 4th order Runge-Kutta method was used for advancing in time. We simulated Eqs. (4), (5), (9), and (10) with the added hyperviscosity term $-D_{4v} \frac{\partial^4 f_i}{\partial v_z^4}$ into the right-hand side of (4), where $D_{4v}$ is the hyperviscosity coefficient typically chosen $D_{4v} = 10^{-8}$. At each time step, we filtered out all Fourier modes of $\{u_i\}_{i=1\ldots N}$ in $x$ and $z$ with $\theta > \theta_{max} = 0.65$ to suppress the unphysical two-stream instability of VMD (see also Sec. III).

Initial distributions were uniform in space and Gaussian in $v_z$ direction for each flow: $f_i|_{t=0} = (2\pi)^{-1/2} e^{-v_z^2/2} \rho_i|_{t=0}$, $i = 1\ldots N$. The transverse VMD flows with velocities $\{u_i\}_{i=1\ldots N}$ and densities $\{\rho_i\}_{i=1\ldots N}$ were chosen in initial conditions to satisfy (16) and (17) as explained in Sec. III as well as to have a zero mean velocity in the transverse direction. These are exact solutions of the Vlasov Eq. (3) as explained in Sec. II. To obtain nontrivial dynamics beyond this time-independent solution, we use an external pump at the beginning of simulation. That initial pumping of the system was done by applying the external electrical field determined from the electrostatic potential $\phi_{ext}$ as follows:

$$\phi_{ext} = 0.009 P(t) \cos(kz - \omega_0 t) \exp[-(x/a)^2],$$
$$(E_{x,ext}, E_{z,ext}) = -\nabla \phi_{ext}, \qquad (24)$$

where $E_{x,ext}$, $E_{z,ext}$ are the longitudinal and transverse components of the electric field, respectively, $\omega_0 = 1.2$, $k = 1/3$, $a = 532/(2\ln 2)^{1/2}$, and $P(t)$ is the time-dependent amplitude. $P(t)$ is chosen, similar to Ref. 23, to grow smoothly from zero to 1 at the time interval $(0, 2\pi/\omega_0)$, then, it stays 1 at $2\pi/\omega_0 < t < 100$ and decays smoothly to zero at $100 < t < 100 + 2\pi/\omega_0$. For all larger times, $P(t)$ is zero. The differences in our simulation settings in comparison with Ref. 2 for (24) are that: (a) we used the Gaussian profile $\exp[-(x/a)^2]$ instead of $cos^2(2\pi x/3200)$ of Ref. 2 and (b) we took into account $E_{x,ext}$ so that the external electric field in (24) satisfies the electrostatic condition $\nabla \cdot E_{ext} = 0$, while Ref. 2 set $E_{x,ext} \equiv 0$. Ref. 2 also performed PIC simulations with the same type of the Gaussian transverse profile as we did; however, no detailed result of PIC simulations was given in Ref. 2 (except integral quantities) so that only comparison with the Vlasov simulation results of Ref. 2 is possible.

To imitate outgoing boundary conditions in $x$ direction, as in Ref. 2, a smoothing filtering at the boundaries in $x$-direction was used by adding $-[f_i - f_i(0)]G(x)$ term to the right-hand side of (4) and $-[u_i - u_i(0)]G(x)$ term to the right-hand side of (5). Here, $G(x) = (2^{15}65/L_x)(x/L_x)^{12}$ insures the hyperexponential convergence of of $f_i$ to $f_i(0)$ and $u_i$ to $u_i(0)$ for $x \to \pm L_x/2$ for all times. Also, $f_i(0) = (2\pi)^{-1/2} e^{-v_z^2/2} \rho_i|_{t=0}$ is the initial Maxwellian distribution and $u_i(0) = u_i|_{t=0}$ are the initial velocities of the transverse flows. Thus, the simulations are periodic but adding filtering near boundaries suppresses (in about 16 orders of magnitude) the periodic return of exiting electrons back to the system.

Figure 16 shows the time dependence of the maximum of $\max_z |E_z(x = 0, z, t)|$ (the maximum of $|E_z|$ vs. $z$ at the center $x = 0$ in the transverse direction) for different numbers of flows $N$ and hyperviscosity $D_{4v}$. It is seen that the decrease of hyperviscosity results in the moderate increase of the amplitude of the peak at $t \simeq 1500$. Figures 17 and 18 show the density plot for $\langle E_z^2 \rangle_z \equiv L_z^{-1} \int_0^{L_z} E_z^2 dz$ ($E_z^2$ averaged over $z$) in $(t, x)$ plane for $N = 2$ and $N = 21$, respectively. It is seen from comparison of Figures 17 and 18 that in both cases $\langle E_z^2 \rangle_z$ self-focuses in $x$ as time progresses, similar to that observed in Vlasov simulations of Ref. 2. After the focus,

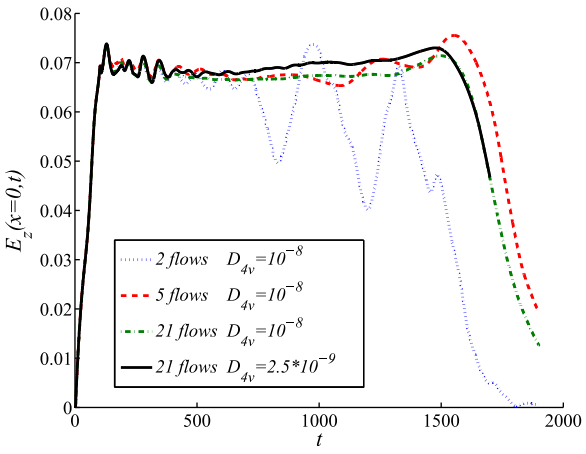


FIG. 16. The time dependence of the maximum of $\max_z |E_z(x = 0, z, t)|$ for 2, 5, and 21 flows and different values of the hyperviscosity $D_{4v}$.

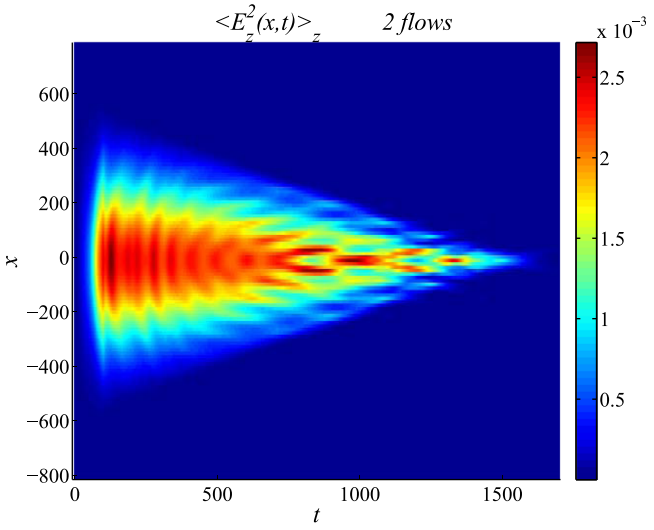


FIG. 17. The density plot for $\langle E_z^2 \rangle_z \equiv L_z^{-1} \int_0^{L_z} E_z^2 dz$ for $N = 2$ flows.

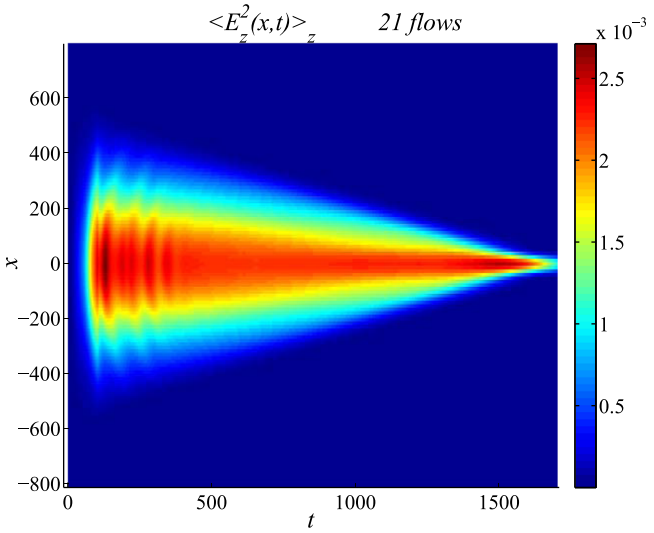


FIG. 18. The density plot for $\langle E_z^2 \rangle_z \equiv L_z^{-1} \int_0^{L_z} E_z^2 dz$ for $N = 21$ flows.

the field energy is rapidly depleted. However, the important difference between Figures 17 and 18 is that the 2-flow case of Figure 17 also shows the development of transverse instability at intermediate times. That instability significantly weakens the achieved maximum value of $\langle E_z^2 \rangle_z$ in Figure 17 in comparison with 21-flow case of Figure 18. That transverse instability is an artifact of VMD and is suppressed with increase of the number of flows. That instability is also revealed in the oscillations of $\max_z |E_z(x = 0, z, t)|$ in Figure 16, which decrease with increase of the number of flows. Thus, the increase of the number of flow in VMD is necessary in practical simulations until convergence is reached to well approximate the solution of the full Vlasov equation.

## VII. CONCLUSION

In conclusion, we investigated the regions of stability of 2*D* and 3*D* VMD dispersion relations, Eqs. (18) and (22), respectively. We found that with increase of the number of flows, $N$, these regions quickly converge to universal curves in $(k\lambda_D, \theta)$ plane. For $k\lambda_D \lesssim 1$, the maximum stable angle is limited to $\theta \lesssim 0.65$. The dependence of these results on the azimuthal angle $\varphi$ in 3*D* is very weak.

We also studied the relative error between Langmuir wave branch of the VMD dispersion relations (18) and (22) and the exact Langmuir wave dispersion relation (14) of the Vlasov equation. We found that both in 2*D* and 3*D*, these errors are small provided $k\lambda_D \gtrsim 0.3$ and $\theta \lesssim 0.3$. We also found that in 3*D*, a moderate number of flows, $N \geq 6$, already allows us to approximately recover for $\theta \lesssim 0.3$, the isotropy of the LW dispersion relation with high precision.

## ACKNOWLEDGMENTS

The authors would like to acknowledge R. L. Berger for helpful discussion on 2D Vlasov simulations. This work was supported by the National Science Foundation under Grant Nos. PHY 1004118 and PHY 1004110.

[1]A. A. Vlasov, Sov. Phys. Usp. **10**, 721 (1968) [Zh. Eksp. Teor. Fiz. **8**, 291 (1938)].
[2]B. J. Winjum, R. L. Berger, T. Chapman, J. W. Banks, and S. Brunner, Phys. Rev. Lett. **111**, 105002 (2013).
[3]J. M. Dawson, Rev. Mod. Phys. **55**, 403 (1983).
[4]C. K. Birdsall and A. B. Langdon, *Plasma Physics via Computer Simulation* (Taylor & Francis, New York, 2005).
[5]L. Yin, B. J. Albright, K. J. Bowers, W. Daughton, and H. A. Rose, Phys. Rev. Lett. **99**, 265004 (2007).
[6]L. Yin, B. J. Albright, K. J. Bowers, W. Daughton, and H. A. Rose, Phys. Plasmas **15**, 013109 (2008).
[7]L. Yin, W. Daughton, B. J. Albright, K. J. Bowers, D. S. Montgomery, J. L. Kline, J. C. Fernandez, and Q. Roper, Phys. Plasmas **13**, 072701 (2006).
[8]H. X. Vu, D. F. DuBois, D. A. Russell, and J. F. Myatt, Phys. Plasmas **17**, 072701 (2010).
[9]L. Landau, J. Phys. (USSR) **10**, 25 (1946).
[10]D. F. DuBois and M. V. Goldman, Phys. Rev. Lett. **14**, 544 (1965).
[11]D. Montgomery and I. Alexeff, Phys. Fluids **9**, 1362 (1966).
[12]D. A. Russell, D. F. DuBois, and H. A. Rose, Phys. Plasmas **6**, 1294 (1999).
[13]H. A. Rose and W. Daughton, Phys. Plasmas **18**, 122109 (2011).
[14]H. A. Rose, Phys. Plasma **12**, 012318 (2005).
[15]I. B. Bernstein, J. M. Greene, and M. D. Kruskal, Phys. Rev. **108**, 546 (1957).
[16]B. D. Fried, M. Gell-Mann, J. D. Jackson, and H. W. Wyld, J. Nucl. Energy, Part C **1**, 190 (1960).
[17]D. R. Nicholson, *Introduction to Plasma Theory* (Wiley, New York, 1983).
[18]J. Dawson, Phys. Fluids **4**, 869 (1961).
[19]U. Frisch, B. Hasslacher, and Y. Pomeau, Phys. Rev. Lett. **56**, 1505 (1986).
[20]J. P. Holloway and J. J. Dorning, Phys. Rev. A **44**, 3856 (1991).
[21]M. Buchanan and J. Dorning, Phys. Rev. E **52**, 3015 (1995).
[22]H. A. Rose and L. Yin, Phys. Plasmas **15**, 042311 (2008).
[23]J. W. Banks, R. L. Berger, S. Brunner, B. I. Cohen, and J. A. F. Hittinger, Phys. Plasmas **18**, 052102 (2011).